

SCIENTIFIC REPORTS



OPEN

Noise-tunable nonlinearity in a dispersively coupled diffusion-resonator system using superconducting circuits

Received: 26 August 2016
Accepted: 19 December 2016
Published: 25 January 2017

Christin Rhén & Andreas Isacsson

The harmonic oscillator is one of the most widely used model systems in physics: an indispensable theoretical tool in a variety of fields. It is well known that an otherwise linear oscillator can attain novel and nonlinear features through interaction with another dynamical system. We investigate such an interacting system: a superconducting LC-circuit dispersively coupled to a superconducting quantum interference device (SQUID). We find that the SQUID phase behaves as a classical two-level system, whose two states correspond to one linear and one nonlinear regime for the LC-resonator. As a result, the circuit's response to forcing can become multistable. The strength of the nonlinearity is tuned by the level of noise in the system, and increases with decreasing noise. This tunable nonlinearity could potentially find application in the field of sensitive detection, whereas increased understanding of the classical harmonic oscillator is relevant for studies of the quantum-to-classical crossover of Jaynes-Cummings systems.

The harmonic oscillator is one of the most well-understood dynamical systems in physics, and is used as a model in nearly every field. The classical harmonic oscillator was studied already by Galileo Galilei, while its quantum counterpart was described in 1925 by Paul Dirac. It remains one of few models that can be exactly solved, and as such, it features prominently in courses on classical and quantum mechanics. It is perhaps surprising, then, that the harmonic oscillator still remains at the forefront of contemporary physics research.

Today, considerable attention is devoted to harmonic oscillators that interact with an auxiliary dynamical system. This situation appears, for instance, in circuit quantum electrodynamics^{1–3} and quantum information processing^{4–8}, where the harmonic oscillator models a superconducting microwave circuit and the auxiliary system is a qubit. Then, manipulation of the circuit allows for control and read-out of the state of the qubit. In a similar manner, when the auxiliary system is a second harmonic oscillator, as in optomechanics^{9–12}, one of the oscillators can be damped or driven by manipulating the other.

A case that exhibits a variety of intriguing, nonlinear effects is when another very common model system takes the role of auxiliary system: the diffusing Brownian particle. One proposed realization of such a coupled system is a diffusing particle loosely adsorbed on the surface of a nanomechanical resonator^{13–17}. Then, the particle position directly influences the oscillator's natural frequency, and the oscillator in turn provides an amplitude-dependent inertial back-action force on the particle. Despite its apparent simplicity, this diffusion-resonator system exhibits surprising effects such as induced nonlinearity¹³ and bistability¹⁴, inhomogeneous dephasing¹⁵, as well as mode coupling and non-linear dissipation^{16,17}. As shown recently¹⁸, these features are rather generic for a harmonic oscillator mode coupled dispersively to an auxiliary dynamical system, under certain circumstances. However, with the current state of the art, it is very difficult to fabricate this nanomechanical system in a parameter regime where an interesting physical response will be observable.

Here we propose an alternative realization of a resonator-diffusion system, making use of superconducting circuit elements. These allow for a high degree of control over the relevant parameters, some of which can be tuned *in situ*. Our proposed realization, depicted in Fig. 1(a), makes use of a resistively shunted superconducting quantum interference device (SQUID), whose phase variable will act as a diffusing particle due to the presence of noise in the shunting resistor. The harmonic oscillator is represented by a lumped superconducting LC-resonator,

Chalmers University of Technology, Department of Physics, SE-412 96 Göteborg, Sweden. Correspondence and requests for materials should be addressed to C.R. (email: christin.rhen@chalmers.se)

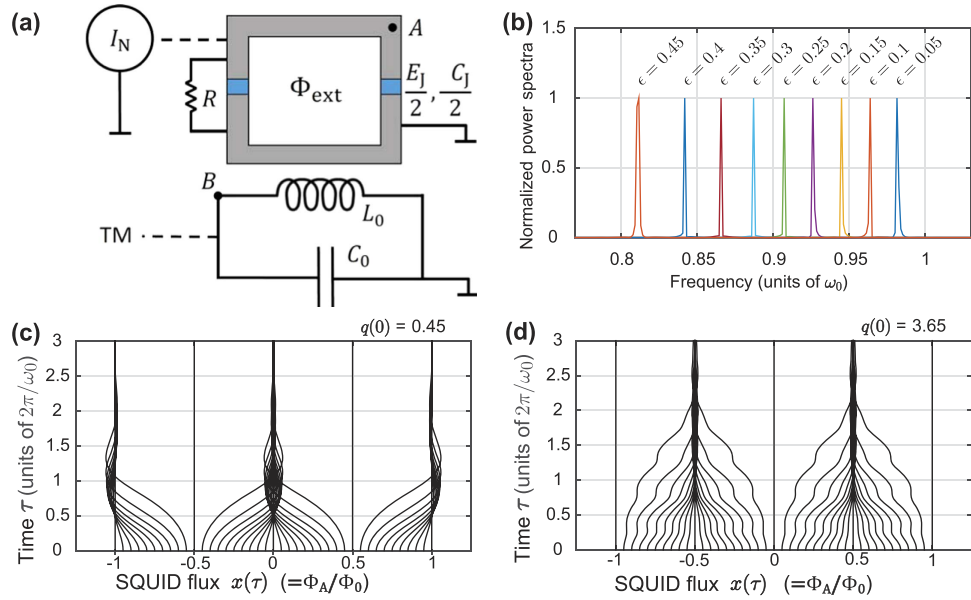


Figure 1. (a) Superconducting circuit realization of a diffusion-resonator system. A symmetric SQUID is inductively coupled to a lumped LC-resonator. A weak inductive coupling ensures a dispersive interaction between the two systems. Additional noise can be introduced in the system using an external noise current source I_N . For read-out and actuation, the LC-resonator can be coupled inductively or capacitively to an external transmission line. The nodes A and B indicate where the node fluxes used below as dynamic variables are defined. (b)–(d) Numerical integration of the full equations of motion (5)–(6), absent external drive and noise ($f(\tau) = 0, \gamma = 0, \eta = 0$, and $\mathcal{D} = 0$). (b) Resonator power spectra for increasing coupling ϵ . The phase of the SQUID is rapidly trapped at integer (c) or half-integer (d) values of x , depending on resonator amplitude. Note that the quite large values of ϵ used in (b) are chosen to illustrate the frequency shift clearly; the $\epsilon = 0.01$ used in (c)–(d) would correspond to a much smaller frequency shift.

and is inductively coupled to the SQUID. We find that when the resonator is driven, the SQUID phase takes one of two equilibrium values; it behaves as a classical two-level system. Interestingly, the LC-circuit exhibits dramatically different dynamics for the two values of the phase. In one case the circuit becomes a linear oscillator, while in the other it is highly nonlinear and can be multistable. As the resonator amplitude increases, the system switches between linear and non-linear regimes in a quasi-periodic manner, determined by the noise level and the drive amplitude. We derive an analytical model that is very successful at predicting the two regimes, and discuss where this model breaks down.

While it is clear that the tunable nonlinearity found in the studied circuit could find application in the field of sensitive detection (c.f. Josephson bifurcation amplifiers¹⁹), our results also have more fundamental implications. In the quantum regime, a two-level system coupled to a harmonic oscillator is described by the well-studied Jaynes-Cummings Hamiltonian. However, an understanding of the transition between this quantum regime and its classical counterpart remains elusive. As we here investigate the *classical* dynamics of a harmonic oscillator coupled to a two-level system, new light is shed on the less-known half of this quantum-to-classical crossover.

Results

Circuit description. We study a system consisting of a symmetric SQUID in the vicinity of a lumped LC-resonator with capacitance C_0 and inductance L_0 , as shown in Fig. 1(a). For actuation and readout purposes, the resonator can be coupled to an external transmission line. Each Josephson junction in the SQUID is characterized by a capacitance $C_J/2$ and Josephson energy $E_J/2$. We take as dynamic variables the fluxes $\Phi_{A,B} \equiv \int_{-\infty}^t dt' V_{A,B}(t')$ at points A and B, respectively, indicated in Fig. 1(a). The conservative dynamics of the system is then described by the Lagrangian

$$L = \frac{1}{2}C_0\dot{\Phi}_B^2 - \frac{1}{2}\frac{\Phi_B^2}{L_0} + \frac{1}{2}C_J\dot{\Phi}_A^2 - E_J \cos \frac{\pi\Phi_{\text{ext}}}{\Phi_0} \left(1 - \cos \frac{2\pi\Phi_A}{\Phi_0} \right), \quad (1)$$

where $\Phi_0 = h/2e$ is the flux quantum. The external flux Φ_{ext} threading the SQUID is partly determined by the current in the LC-circuit. If there are no other sources of external flux, the coupling is linear to lowest order in Φ_B ; $\Phi_{\text{ext}} \approx 2g\Phi_B$. Defining nondimensional variables $q = 2\pi g\Phi_B/\Phi_0$ and $x = \Phi_A/\Phi_0$, Eq. (1) leads to the equations of motion

$$\ddot{q} + \frac{1}{L_0C_0}q - (2\pi g)^2 \frac{E_J}{C_0\Phi_0^2} \sin q(1 - \cos 2\pi x) = 0, \quad (2)$$

$$\ddot{x} + (2\pi)^2 \frac{E_J}{C_J \Phi_0^2} \cos q \sin 2\pi x = 0. \quad (3)$$

The SQUID has a normal total resistance R , arising from either junction-internal resistance or from additional shunting. That is, the equation for x should be supplemented by damping and noise, leading to the equation for the resistively and capacitively shunted Josephson junction (RCSJ) model^{20,21}:

$$\ddot{x} + \frac{1}{RC_J} \dot{x} + (2\pi)^2 \frac{E_J}{\Phi_0^2 C_J} \cos q \sin 2\pi x = \frac{\sqrt{D}}{RC_J} \xi(t). \quad (4)$$

The RCSJ-model has reliably been able to reproduce experimental²² results in regimes where $\hbar\omega_J < k_B T$, with $\omega_J = 2\pi\Phi_0^{-1}\sqrt{E_J/C_J}$ being the plasma frequency.

As noted already by Ambegaokar and Halperin²³, the SQUID phase dynamics is that of a particle executing Brownian motion in a potential. For purely thermal fluctuations, the current noise in the resistive component is given by the Callen-Welton formula $S_{II}(\omega) = (\hbar\omega/\pi R) \coth(\hbar\omega/2k_B T)$. We consider here the classical limit $\hbar \rightarrow 0$, which allows us to treat the noise as Gaussian white noise: $\langle \xi(t)\xi(t') \rangle = \delta(t-t')$ with a diffusion constant given by $D = 2k_B TR/\Phi_0^2$. However, it is also possible to impose noise externally by attaching a noisy current source I_N , as shown in Fig. 1(a).

Rescaling the time variable to dimensionless time $\tau = \omega_0 t$, with $\omega_0 = 1/\sqrt{L_0 C_0}$, the equations of motion reduce to the form

$$\ddot{q} + \gamma \dot{q} + q - \varepsilon \sin q (1 - \cos 2\pi x) = f(\tau) \quad (5)$$

$$\dot{x} + \eta \dot{x} + \alpha \cos q \sin 2\pi x = \eta \sqrt{D} \xi(\tau). \quad (6)$$

Here, we have introduced a finite quality (Q-) factor $1/\gamma$ to the LC-resonator, and added the external drive $f(\tau)$.

The nondimensional constants ε , α , η , and D entering Eqs (5) and (6) are related to physical quantities through

$$\varepsilon \equiv \frac{(2\pi g)^2 E_J}{C_0 \Phi_0^2 \omega_0^2} = \frac{2\pi g^2 I_c}{C_0 \Phi_0 \omega_0^2} = 2\pi g^2 \frac{I_c}{I_0}, \quad (7)$$

$$\alpha \equiv \frac{(2\pi)^2 E_J}{C_J \Phi_0^2 \omega_0^2} = \frac{2\pi I_c}{C_J \Phi_0 \omega_0^2} = 2\pi \frac{C_0 I_c}{C_J I_0}, \quad (8)$$

$$\eta \equiv \frac{1}{C_J R \omega_0}, \quad (9)$$

$$D \equiv \frac{2k_B TR}{\omega_0 \Phi_0^2} = \frac{2k_B T}{I_0 \Phi_0} R C_0 \omega_0 = \frac{T}{T_0}. \quad (10)$$

Here, $I_0 \equiv C_0 \Phi_0 \omega_0^2$ is the characteristic scale for the current through the LC-circuit, and $I_c = 2\pi E_J/\Phi_0$ is the critical current of the junctions. The temperature scale is $T_0 = \Phi_0 I_0 / 2k_B R C_0 \omega_0$.

It should be noted that as the dissipative term $\gamma \dot{q}$ is introduced in Eq. (5), the fluctuation-dissipation theorem dictates that a stochastic force component $f_N = \gamma \sqrt{D} \xi_q(\tau)$ is included in the external force f . This additive noise f_N is proportional to $\gamma = 1/Q$, which, in LC-circuits at cryogenic temperatures, can easily be as small as $10^{-5} - 10^{-6}$. Even for the comparably bad LC-resonator (with $\gamma = 10^{-3}$) used in our simulations, the effect of the flux-noise term in Eq. (6) is an order of magnitude larger than that from f_N with the parameters used here.

Parameter values. We consider a typical LC-circuit with $L_0 = 1$ nH and $C_0 = 0.1$ pF, corresponding to an LC-frequency of $\omega_0 = (L_0 C_0)^{-1/2} = 10^{11}$ s⁻¹. The resulting characteristic current scale for the LC-circuit is $I_0 = 2 \mu$ A. We further consider junctions with Josephson energy $E_J = 0.6$ meV and capacitance $C = 1$ pF, shunted by a resistance $R = 16 \Omega$. Using an external shunt resistance, I_c becomes largely independent of R , and can be tuned by the temperature; here, we have $I_c = 0.5 \mu$ A at a temperature $T = 3$ K. These parameter values, along with the resulting dimensionless parameters, are listed in Table 1.

For the nondimensional coupling constant g between the SQUID and the resonator we use $g = 0.1$, and set the LC-resonator inverse Q-factor to $\gamma = 0.001$. The relatively large values of g and γ were chosen for computational convenience. As will be seen in the analysis below, for weaker coupling g the same response will occur provided the resonator damping γ is reduced accordingly.

We will consider a periodic driving force $f(\tau) = f_0 \cos \Omega \tau$, where f_0 is dimensionless. In practice, this coefficient is related to the number of drive photons. The mean photon occupancy of the LC-resonator is

Physical parameters				Dimensionless quantities	
T_0	1000 K	E_j	0.6 meV	γ	0.001
L_0	1 nH	R	16 Ω	ε	0.015
C_0	0.1 pF	C_j	1 pF	α	0.15
ω_0	100 GHz	ω_j	3 GHz	η	0.625
I_0	2 μ A	I_c	0.5 μ A	\mathcal{D}	0.003

Table 1. Typical values for circuit parameters, and the corresponding dimensionless parameters. The simulation temperature T was chosen as 3 K, and the Q-factor of the LC-resonator was set to 1000.

$$n_{\text{ph}} = \frac{\langle E_{\text{LC}} \rangle}{\hbar\omega_0} = \frac{\langle q^2 \rangle \Phi_0^2}{8\pi^2 g^2 \hbar} \sqrt{\frac{C_0}{L_0}} = \frac{f_0^2 \Phi_0^2}{16\pi^2 g^2 \gamma^2 \hbar} \sqrt{\frac{C_0}{L_0}}, \quad (11)$$

where the resonator energy $E_{\text{LC}} = \Phi_B^2/2L_0$ and $\langle q^2 \rangle = f_0^2/2\gamma^2$ for an unperturbed resonator ($\varepsilon = 0$) driven at resonance. Substitution of the parameter values of Table 1 yields $n_{\text{ph}} \approx 10f_0^2/\gamma^2$. For an inverse Q-factor $\gamma = 10^{-3}$ and drive amplitudes $f_0 \simeq 10^{-2}$, we thus find $n_{\text{ph}} \approx 10^3$.

Equivalence with nanomechanical system. To connect Eqs (5)–(6) to the nanomechanical resonator-physical particle system studied in refs 13–17, we note that for a small amplitude $|q| \ll 1$, Equations (5) and (6) resemble the equations of motion of a particle diffusing on a vibrating string. Expanding the trigonometric terms and identifying the vibrational mode function $\varphi(x) = \sqrt{2} \sin \pi x$, we find

$$\ddot{q} + \gamma \dot{q} + [1 - \varepsilon \varphi^2(x)]q = f(\tau) \quad (12)$$

$$\ddot{x} + \eta \dot{x} + \frac{\alpha}{2\pi} \partial_x [\varphi^2(x)](1 - q^2/2) = \eta \sqrt{\mathcal{D}} \xi(\tau). \quad (13)$$

This is exactly the single-mode equations of motions seen in ref. 16, with the addition that the unperturbed ($q = 0$) motion of the particle described by x is no longer free diffusion. Instead, the unperturbed SQUID phase is affected by a spatial potential proportional to $\varphi^2(x)$. For $q \neq 0$, x thus moves in an effective potential given by the combination of this spatial potential, and of the q -dependent “inertial” potential created by the resonator oscillation. With this addition taken into account, the nanomechanical system and the superconducting circuit show the same dynamics; the presence of a “particle” causes the frequency of the LC-resonator to shift downwards, as shown in Fig. 1(b), while the resonator motion causes trapping of the particle, see Fig. 1(c–d).

Linear and nonlinear regimes. In the superconducting circuit, the total effective potential that determines the dynamics of the SQUID flux x is a combination of the effective potential created by the oscillation in the LC-circuit, that traps the flux near $x_{\text{eq}} = n + 1/2$, $n \in \mathbb{Z}$, and a spatial potential proportional to $\sin^2 \pi x$, that traps the flux near $x_{\text{eq}} = n$. The steady-state value x_{eq} thus depends on the relative strength of these two effects, which is determined by the resonator amplitude; see Fig. 1(c–d).

This interaction of two periodic potentials causes the resonator-SQUID system to display very interesting action-backaction dynamics. The resonator amplitude determines the equilibrium position x_{eq} of the flux particle. Both integer and half-integer x_{eq} have in common that the supercurrent through the SQUID, $I_s = I_c \cos q \sin 2\pi x$, vanishes, and Eq. (6) reverts to the familiar Langevin equation. However, the value of x has a dramatic impact on the dynamics of the resonator, tuning it from linear to highly nonlinear depending on whether x_{eq} is integer or half-integer.

When x is an integer, the term proportional to ε in Eq. (5) vanishes, and the equation for the LC-resonator becomes that of a driven damped linear oscillator. As such, it should exhibit a Lorentzian frequency response with maximum at f_0/γ and width γ . When x is a half-integer, the absolute value of the ε -term is maximized; this is the maximally non-linear regime. For $f_0 = 0$ and $x = n + 1/2$, Eq. (5) becomes $\ddot{q} + \gamma \dot{q} + q = 2\varepsilon \sin q$, which describes an inverted physical pendulum of the kind used in the Holweck-Lejay gravimeter²⁴.

Driven response. We now turn to the driven response by considering a periodic driving force $f(\tau) = f_0 \cos \Omega \tau$. The resonator amplitude will depend on the drive amplitude and frequency, and the value of x will in turn depend on the resonator oscillation.

First, we analytically estimate the system’s response to the drive by analyzing it in the adiabatic, mean-field, rotating wave approximation. The full stochastic equations of motion are then numerically solved. Except for in a small region of anomalous response, the agreement between the analytical and numerical solutions is excellent.

Adiabatic RWA solution. To find the steady-state solution of the slow-moving envelope $|u|$ of the resonator oscillation, we make the change of variables $2q = (ue^{i\Omega\tau} + u^*e^{-i\Omega\tau})$, $2\dot{q} = i\Omega(ue^{i\Omega\tau} - u^*e^{-i\Omega\tau})$. In the rotating wave approximation (RWA), the equations of motion (5)–(6) transform into

$$\dot{u} = \left[-\frac{\gamma}{2} + i \left(\frac{\varepsilon \varphi^2(x)}{|u|} J_1(|u|) - \sigma \right) \right] u + \frac{f_0}{2i}, \tag{14}$$

$$\ddot{x} + \eta \dot{x} + \frac{\alpha}{2\pi} J_0(|u|) \partial_x [\varphi^2(x)] = \eta \sqrt{\mathcal{D}} \xi(\tau). \tag{15}$$

Here, we have assumed that the detuning $\sigma = \Omega - 1$ is small ($|\sigma| \ll 1$), and we use $\varphi(x) = \sqrt{2} \sin \pi x$ for brevity. Additionally, $J_{0,1}$ are Bessel functions of the first kind. Note that the coupling constant g only affects ε in Eq. (14), and that a change in ε can be compensated for by a corresponding change in damping γ .

The dynamics captured by Eqs (14)–(15) can also be described by the equivalent Fokker-Planck equation²⁵ (FPE):

$$\begin{aligned} \partial_\tau p = & -\partial_u \left[-\frac{\gamma}{2} u p + i \left(\frac{\varepsilon \varphi^2(x)}{|u|} J_1(|u|) - \sigma \right) u p \right] \\ & -\partial_{u^*} \left[-\frac{\gamma}{2} u^* p - i \left(\frac{\varepsilon \varphi^2(x)}{|u|} J_1(|u|) - \sigma \right) u^* p \right] \\ & -\partial_x [\dot{x} p] - \partial_{\dot{x}} \left[-\eta \dot{x} p - \frac{\alpha}{2\pi} J_0(|u|) \partial_x [\varphi^2(x)] p \right] + \frac{1}{2} \partial_{\dot{x}}^2 [\eta^2 \mathcal{D} p], \end{aligned} \tag{16}$$

where $p = p(u, u^*, x, \dot{x}, \tau)$ is the system probability density in state space. In the adiabatic limit, in which the relaxation time of the SQUID flux dynamics is much shorter than the relaxation time of the resonator ($\gamma \ll \eta$), the system state can be approximately described by a quasi-stationary probability distribution $p_{st.}(x, \dot{x}, |u|)$. By treating the slow variable $|u|$ as a constant, we find from Eq. (16) that $p_{st.}$ is the solution of

$$-\partial_x [\dot{x} p_{st.}] - \partial_{\dot{x}} \left[-\eta \dot{x} p_{st.} - \frac{\alpha}{2\pi} J_0(|u|) \partial_x [\varphi^2(x)] p_{st.} \right] + \frac{1}{2} \partial_{\dot{x}}^2 [\eta^2 \mathcal{D} p_{st.}] = 0. \tag{17}$$

This can be interpreted as the equation of motion for a system described by the (non-dimensionalized) Hamiltonian $H = \frac{1}{2} \dot{x}^2 + \frac{\alpha}{2\pi} J_0(|u|) \varphi^2(x)$, connected to a reservoir with dimensionless temperature $\eta \mathcal{D} / 2$. It follows that

$$p_{st.}(x, \dot{x}, |u|) = \frac{1}{Z} \exp \left[-\frac{\dot{x}^2}{\eta \mathcal{D}} - \frac{\alpha}{\pi \eta \mathcal{D}} J_0(|u|) \varphi^2(x) \right], \tag{18}$$

where $Z = \sqrt{\eta \mathcal{D} \pi} \exp \left[-\frac{\alpha}{\pi \eta \mathcal{D}} J_0(|u|) \right] I_0 \left(\frac{\alpha}{\pi \eta \mathcal{D}} J_0(|u|) \right)$, and I_0 is the modified Bessel function of the first kind.

We now make the mean-field approximation $\varphi^2 \rightarrow \langle \varphi^2 \rangle = \int p_{st.}(x) \varphi^2(x) dx$, and solve for the stationary solution of Eq. (14). The result is that the stationary amplitude $|u|$ is determined by

$$|u|^2 \left[\frac{\gamma^2}{4} + [\sigma - \varepsilon h(|u|)]^2 \right] = \frac{f_0^2}{4}, \tag{19}$$

where the frequency shift $h(|u|)$ is given by

$$h(|u|) = \frac{J_1(|u|)}{|u|} \left[\frac{I_1(J_0(|u|) \alpha / \pi \eta \mathcal{D})}{I_0(J_0(|u|) \alpha / \pi \eta \mathcal{D})} - 1 \right]. \tag{20}$$

Interestingly, only the ratio $\alpha / \pi \eta \mathcal{D} = I_c \Phi_0 / k_B T = 2 I_c \Phi_0 / R S_0$ (where $S_H(\omega) = S_0$ for white noise) enters into the expression for the scaled frequency shift $h(|u|)$. This ratio can also be written as $2\pi E_J / k_B T$. In other words, the frequency shift, and hence the qualitative dynamics of the system, is determined by the ratio between the Josephson energy and the thermal energy.

In Fig. 2(a), the frequency shift $h(|u|)$ is shown for four different values of this ratio. For low resonator amplitudes (small $|u|$), the resonant frequency shifts downwards upon increasing the noise. As amplitude increases, either softening or hardening is observed depending on the noise power. The function h has an infinite number of crossings with the horizontal axis, tending to zero as $|u|^{-3/2}$ in the limit of large $|u|$. The overall shape of the resonance curve, shown in the inset of Fig. 2(a), can be understood from treating the limits of high and low noise.

In the low noise limit, $\mathcal{D} \rightarrow 0$, the ‘‘particle’’ coordinate x will localize at integer values ($x = n$) if $J_0(|u|) > 0$, and at half-integer values ($x = n + 1/2$) if $J_0(|u|) < 0$. The SQUID phase thus behaves as a classical two-level-system (TLS), whose state depends on the amplitude of the resonator. In this limit, the frequency shift $h(|u|)$ approaches $2[\theta(J_0(|u|)) - 1]J_1(|u|)/|u|$. Hence, the zeros of J_0 separate regions where the oscillator response is shifted away from the unperturbed Lorentzian line shape and regions where the two coincide: between regions where the LC-circuit has ordinary linear behavior and regions where it behaves as a driven Holweck-Lejay-like resonator.

As noise increases, one sees from Fig. 2(a) that the sharp features of the frequency shift $h(|u|)$ are smoothed out, so that $h(|u|)$ only vanishes at those discrete amplitudes $|u|$ that correspond to zeros of J_1 . Hence, in the

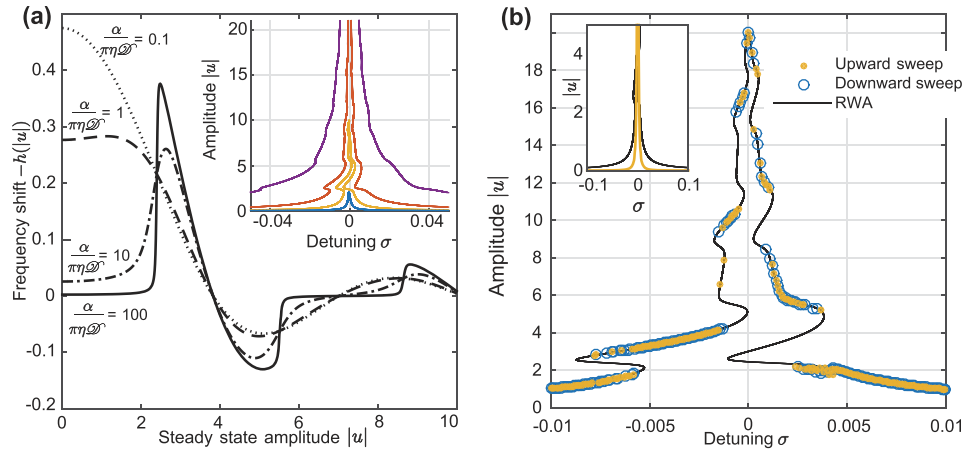


Figure 2. (a) Frequency shift $h(|u|)$ as function of amplitude $|u|$ in the adiabatic, mean-field, rotating wave approximation for different values of the ratio $\alpha/\pi\eta D$. In the low noise limit (solid curve), for small $|u|$ the phase particle is trapped at integer x , resulting in a zero frequency shift. For larger diffusion, the resonant frequency at low amplitudes increases with increasing noise (D). The inset shows the corresponding frequency response curves as a function of detuning $\sigma = \Omega - 1$, obtained by solving Eq. (19). Here, $\alpha/\pi\eta D = 25$, as given by the parameter values in Table 1, and we consider drive amplitudes $f_0 = 0.002$ (blue curve), $f_0 = 0.01$ (yellow curve), $f_0 = 0.04$ (red curve), and $f_0 = 0.2$ (purple curve). For moderate drive amplitudes $f_0 \lesssim \varepsilon$, multistability beyond bistability is possible. (b) Simulated resonant response of the circuit, as the drive frequency is swept up (yellow dots) and down (blue circles). The black curve is the analytical response; the agreement is excellent. Here, the drive amplitude $f_0 = 0.02$, and $\alpha/\pi\eta D = 25$. Since temperature is finite, there is noise-induced switching between multistable states, and hysteresis loops are smeared. The inset shows the bottom of the resonant peak (black) together with the Lorentzian response of an unperturbed system (yellow) – broadening is significant.

presence of non-negligible noise the piecewise linear behavior in $|u|$ obtained for $D = 0$ is destroyed, and for strong noise $h(|u|) \rightarrow -J_1(|u|)/|u|$. We conclude that by varying the noise intensity, the frequency response can be tuned.

The shape of the response curve is also influenced by the drive strength. As expected, and also shown in the inset of Fig. 2(a), the resonance peak looks Lorentzian for small f_0 , but quickly takes on a flame-like character as the driving force increases. However, as the drive amplitude increases further, the response once more resembles a Lorentzian. This return to apparent linearity can again be traced back to the structure of the frequency detuning function $h(|u|)$, which decays algebraically with $|u|$. Consequently, the frequency shift near the top of the resonance peak quickly decays with increasing f_0 . At the base of the resonance, on the other hand, the width of the peak is of order $f_0/|u|$, whereas the frequency detuning scales with ε . Hence, we expect no visible nonlinear response when $f_0 \gtrsim \varepsilon$.

Frequency response. The stochastic equations of motion (5)–(6) were numerically integrated using a second-order algorithm^{26,27}, with the parameter values listed in Table 1. These correspond to $\alpha/\pi\eta D = 25$.

To begin with, the resonant response of the LC-circuit was calculated. The drive frequency Ω was varied while $f_0 = 0.02$, and the corresponding amplitude response found; the results are shown in Fig. 2(b). The agreement between simulation and the analytical results above is excellent.

In order to further check the validity of the RWA-analysis above, we extracted the distribution of $x(\tau)$ for states stabilized at a certain envelope amplitude $|u|$. The result is shown in Fig. 3(a), where switching between integer and half-integer x_{eq} is clearly evident. The sections where no values are plotted are those $|u|$ where no stable state could be found, due to that $\partial|u|/\partial\sigma \rightarrow \infty$. For comparison, Fig. 3(b) includes the theoretical response curve together with the Lorentzian $f_0\gamma^{-1}(1 + \sigma^2/\gamma^2)^{-1}$. In agreement with the discussion above, there is a clear correspondence between integer x_{eq} and regions where the resonance curve is very close to the unperturbed Lorentzian, whereas half-integer x_{eq} coincide with highly nonlinear resonant response.

Due to the presence of thermal noise, in Fig. 2(b) expected hysteresis loops are smeared and there is very little difference between frequency sweeps up and down. Instead, the existence of multistability is proven by making a large number of measurements at the same detuning. To that end, several hundred trajectories were calculated, and the final resonator amplitude was recorded in each case. The initial state $(q(0), \dot{q}(0), x(0), \dot{x}(0))$ of the system was given by four random numbers, each uniformly distributed in the interval $(-10, 10)$. The result is shown in Fig. 3(c); the existence of multistability is clearly evident. Here, the considered values for the detuning σ were chosen to be such that the theoretical resonance curve indicates that several stable states might occur, as shown in the inset of Fig. 3(c).

The time evolution for the resonator amplitude and the SQUID phase is shown in, respectively, Fig. 3(d) and (e). Here, the detuning $\sigma = -0.0013$, and the initial state of the system is $x(0) = 0.25$, $\dot{x}(0) = \dot{q}(0) = 0$, while $q(0)$ is, respectively, 2.4, 2.6, and 3.0. As a consequence of the multistable response to driving, these small

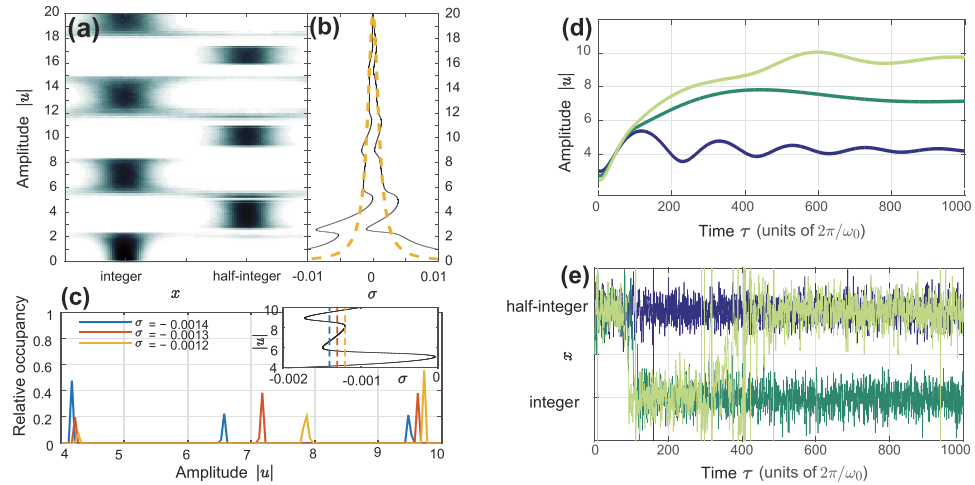


Figure 3. (a) Distribution of the SQUID phase x (mapped to the interval $[-\frac{1}{4}, \frac{3}{4}]$) as a function of resonator amplitude $|u|$. (b) Theoretical response curve (solid black line) together with the unperturbed Lorentzian response (yellow dashed line). When x is an integer, the resonator decouples from the SQUID, and the resonator response is very close to the Lorentzian. For half-integer x , the magnitude of the coupling to the SQUID is maximized, and the resonator response is highly non-linear. (c) Distribution of resonator amplitudes for three values of the detuning σ . The inset shows a close-up of the relevant region of the analytical resonance curve, where the dashed lines indicate the examined values of σ . For a given detuning and drive power, three different amplitudes can be observed. (d) Three examples of the time evolution of $|u|$ for $\sigma = -0.0013$. Despite quite small variations in the initial conditions, the system eventually settles in very different states. (e) The corresponding time evolutions of x . In each case, the SQUID phase is initially trapped at a half-integer value. The subsequent evolution of x_{eq} is dictated by the resonator amplitude $|u|$, in agreement with (a).

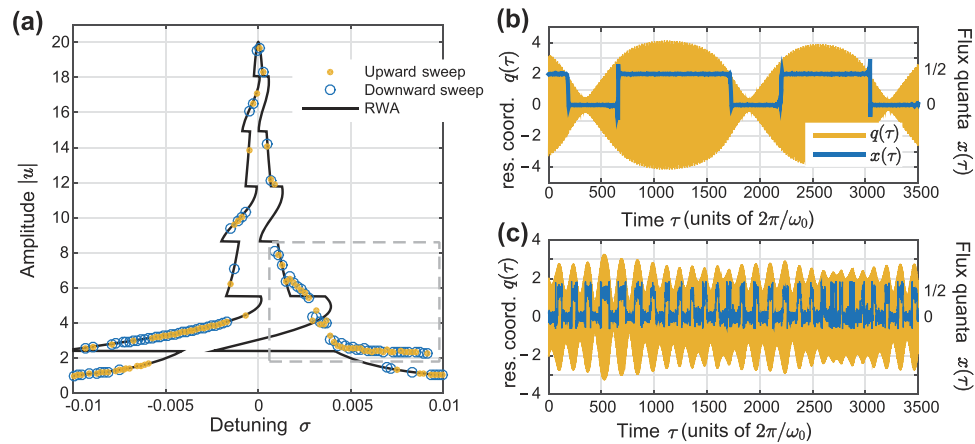


Figure 4. (a) Resonant response at $T \rightarrow 0$ K. The transitions between linear and nonlinear regimes are much sharper than in the case of finite temperatures. The dashed box indicates the anomalous region of detuning σ , where analytical and numerical results do not coincide. (b)–(c) Time evolution for the LC-resonator amplitude q and the SQUID flux x , at $\sigma = 0.003$ and (b) $T \rightarrow 0$ K (c) $T = 3$ K. The response in the anomalous region is non-stationary, with resonator amplitude beats caused by x switching between integer and half-integer values.

variations in initial amplitude can have a dramatic impact on the state in which the LC-circuit eventually settles. Indeed, Fig. 3(d) shows that all three states indicated in Fig. 3(c) do occur. In each case, the state of the x -TLS is governed by the amplitude $|u|$, as shown in Fig. 3(e). The phase is initialized equidistantly from the two x_{eq} , but is trapped near $x_{\text{eq}} = 1/2$ within a few resonator cycles. Once trapped, the dynamics of the phase remains that of Brownian motion in a potential well, but the position of the well is a function of resonator amplitude. This is particularly clear in the case where $q(0) = 2.4$ (light green line); the resonator amplitude begins in a nonlinear regime, and monotonically increases through a linear region and back to non-linear. At the same time, x switches from being trapped at a half-integer value, to integer trapping, and back to non-integer. Note, however, that while the $|u|$ -evolution is smooth and quite slow, the corresponding shifts between the two x_{eq} are very rapid, illustrating the TLS-character of the SQUID phase x .

Zero-temperature limit. Finally, we consider the limit of millikelvin temperatures, such that $\mathcal{D} \simeq 10^{-6}$. With all other parameters as in Table 1, then $\alpha/\pi\eta\mathcal{D} = 2.5 \times 10^4$. Consequently, the frequency shift $h(|u|)$ exhibits incredibly sharp features for $|u|$ such that $J_0(|u|) \approx 0$. The theoretical resonance curve inherits these sharp features, as can be seen in Fig. 4(a). Still, for a large part of the response curve, the calculated response fits the theoretical curve surprisingly well. The exception is an anomalous region of positive σ , indicated in Fig. 4(a) by a dashed box.

A typical time evolution of the oscillator coordinate q and the flux particle position x for detuning $\sigma = 0.003$ is shown in Fig. 4(b). As can be seen, here in the anomalous part of the response, the system makes quasiperiodic transitions between integer and half-integer values of x , leading to beats in the resonator amplitude. The beats stem from the appearance of transient frequency components at $\varepsilon h(|u|)$. These transients appear whenever a transition from integer to half-integer x occurs, that causes the resonance to abruptly shift downwards. While the system remains at half-integer x it is strongly nonlinear and can mix frequency components. Mixing with the drive at $\Omega \approx 1 - \varepsilon h(|u|)$ then causes a resultant which is on resonance, that consequently drives the oscillator at a shifted frequency, leading to the amplitude beats.

Note that the corresponding phenomena cannot occur for negative detuning $\sigma < 0$. Although the opposite process (half-integer to integer x) will lead to transients with positive frequency components, integer x puts the resonator in the completely linear regime. Frequency mixing is then absent, and no component resurrecting the off-resonant motion can appear. Instead, only transient switching behavior is seen before the system reaches a stationary oscillatory state $\dot{u} = 0$.

This anomalous region of deviation between analytical and numerical results is seen also in Fig. 2(b), but only as less well-fitting data points near $\sigma = 0.003$. In this case, the smoothing of $h(|u|)$ that is caused by the higher temperature makes the dynamics far less dramatic. While driving near $\sigma = 0.003$ will still cause $q(\tau)$ to contain frequency components with negative detuning, thermal noise will smear the resulting amplitude beats, as seen in Fig. 4(c). The time the system spends in the nonlinear regime is thus greatly decreased, and the frequency mixing is limited correspondingly. The higher noise level thus acts to *stabilize* the resonator dynamics. This hints at the presence of stochastic resonance, in the broad sense of “randomness that makes a nonlinearity less detrimental to a signal”²⁸.

Discussion

With superconducting circuit quantum electrodynamics being routinely done in the lab, the proposed system should be readily realized. Although the multistable response will only be visible for a particular range of drive powers, and the nonlinear parts of the resonance peak are very narrow, the current state of the art has matured to the point where detecting both these features is well within reach. A successful verification of the results in this Article would be the first experimental observation of induced nonlinearity in a diffusion-resonator system. Such an observation could stimulate further research into the influence of classical and quantum fluctuations in the interplay between harmonic oscillators and other dynamical systems.

References

1. Abdo, B., Suchoi, O., Schtempluck, O., Blencowe, M. & Buks, E. Intermodulation and parametric amplification in a superconducting stripline resonator integrated with a dc-SQUID. *EPL* **85**, 68001 (2009).
2. Fink, J. M. *et al.* Quantum-to-classical transition in cavity quantum electrodynamics. *Phys. Rev. Lett.* **105**, 163601 (2010).
3. Yamamoto, T. *et al.* Superconducting flux qubit capacitively coupled to an LC resonator. *New J. Phys.* **16**, 015017 (2014).
4. Chiorescu, I. *et al.* Coherent dynamics of a flux qubit coupled to a harmonic oscillator. *Nature* **431**, 159 (2004).
5. Lupascu, A., Verwijs, C. J. M., Schouten, R. N., Harmans, C. J. P. M. & Mooij, J. E. Nondestructive readout for a superconducting flux qubit. *Phys. Rev. Lett.* **93**, 177006 (2004).
6. Irish, E. K., Gea-Banachloche, J., Martin, I. & Schwab, K. C. Dynamics of a two-level system strongly coupled to a high-frequency quantum oscillator. *Phys. Rev. B* **72**, 195410 (2005).
7. Schuster, D. I. *et al.* Resolving photon number states in a superconducting circuit. *Nature* **445**, 515 (2007).
8. Petersson, K. D. *et al.* Circuit quantum electrodynamics with a spin qubit. *Nature* **490**, 380 (2012).
9. Johansson, J. R., Johansson, G. & Nori, F. Optomechanical-like coupling between superconducting resonators. *Phys. Rev. A* **90**, 053833 (2014).
10. Regal, C. A., Teufel, J. D. & Lehnert, K. W. Measuring nanomechanical motion with a microwave cavity interferometer. *Nat. Phys.* **4**, 555 (2008).
11. Thompson, J. D. *et al.* Strong dispersive coupling of a high-finesse cavity to a micromechanical membrane. *Nature* **452**, 72 (2008).
12. Palomaki, T. A., Teufel, J. D., Simmonds, R. W. & Lehnert, K. W. Entangling mechanical motion with microwave fields. *Science* **342**, 710 (2013).
13. Atalaya, J., Isacsson, A. & Dykman, M. I. Diffusion-induced dephasing in nanomechanical resonators. *Phys. Rev. B* **83**, 045419 (2011).
14. Atalaya, J., Isacsson, A. & Dykman, M. I. Diffusion-induced bistability of driven nanomechanical resonators. *Phys. Rev. Lett.* **106**, 227202 (2011).
15. Atalaya, J. Mass loading induced dephasing in nanomechanical resonators. *Journal of Physics C* **24**, 475301 (2012).
16. Edblom, C. & Isacsson, A. Diffusion-induced dissipation and mode coupling in nanomechanical resonators. *Phys. Rev. B* **90**, 155425 (2014).
17. Rhén, C. & Isacsson, A. Particle number scaling for diffusion-induced dissipation in graphene and carbon nanotube nanomechanical resonators. *Phys. Rev. B* **93**, 125414 (2016).
18. Maizelis, Z., Rudner, M. & Dykman, M. I. Vibrating multistability and quantum switching for dispersive coupling. *Phys. Rev. B* **89**, 155439 (2014).
19. Vijay, R., Devoret, M. H. & Siddiqi, I. Invited review article: The Josephson bifurcation amplifier. *Rev. Sci. Instrum.* **80**, 111101 (2009).
20. Stewart, W. C. Current-voltage characteristics of Josephson junctions. *Appl. Phys. Lett.* **12**, 277 (1968).
21. McCumber, D. E. Effect of AC impedance on DC voltage-current characteristics of superconductor weak-link junctions. *J. Appl. Phys.* **39**, 3113 (1968).

22. Blackburn, J. A., Cirillo, M. & Grønbech-Jensen, N. A survey of classical and quantum interpretations of experiments on Josephson junctions at very low temperatures. *Phys. Rep.* **611**, 1 (2016).
23. Ambegaokar, V. & Halperin, B. I. Voltage due to thermal noise in the DC Josephson Effect. *Phys. Rev. Lett.* **22**, 1364 (1969).
24. Couillet, P., Gilli, J.-M. & Rousseaux, G. On the critical equilibrium of the spiral spring pendulum. *Proc. R. Soc. A* **466**, 407 (2009).
25. Gardiner, C. W. *Handbook of Stochastic Methods: For Physics, Chemistry and Natural Sciences*, 2nd Ed. (Springer, 1985).
26. Mannella, R. & Palleschi, V. Fast and precise algorithm for computer simulation of stochastic differential equations. *Phys. Rev. A* **40**, 3381 (1989).
27. Mannella, R. A gentle introduction to the integration of stochastic differential equations in *Stochastic Processes in Physics, Chemistry, and Biology* (ed. Freund, J. A. & Pöschel, T.) 353–364 (Springer, 2000).
28. McDonnell, M. D. & Abbott, D. What is stochastic resonance? Definitions, misconceptions, debates, and its relevance to biology. *PLoS Comput. Biol.* **5.5**, e1000348 (2009).

Acknowledgements

We acknowledge helpful discussions with Prof. Göran Johansson and Prof. Jari Kinaret. This work was supported by the Foundation for Strategic Research SSF (C.R.), the Knut and Alice Wallenberg foundation (C.R.), the Swedish Research Council VR (A.I.), and the Royal Society (International Exchange Grant No. IE140367) (A.I.).

Author Contributions

C.R. and A.I. contributed equally to this work.

Additional Information

Competing financial interests: The authors declare no competing financial interests.

How to cite this article: Rhén, C. and Isacson, A. Noise-tunable nonlinearity in a dispersively coupled diffusion-resonator system using superconducting circuits. *Sci. Rep.* **7**, 41313; doi: 10.1038/srep41313 (2017).

Publisher's note: Springer Nature remains neutral with regard to jurisdictional claims in published maps and institutional affiliations.



This work is licensed under a Creative Commons Attribution 4.0 International License. The images or other third party material in this article are included in the article's Creative Commons license, unless indicated otherwise in the credit line; if the material is not included under the Creative Commons license, users will need to obtain permission from the license holder to reproduce the material. To view a copy of this license, visit <http://creativecommons.org/licenses/by/4.0/>

© The Author(s) 2017